Progress In Electromagnetics Research, Vol. 153, 103–111, 2015

Accurate and Efficient Analysis of Large Antenna Arrays with Radome on a Large Aircraft

Xu-Min Sun, Ming-Lin Yang, and Xin-Qing Sheng*

Abstract—An accurate and efficient computational approach is presented for analyzing radiation characteristics of large antenna arrays with radome. This approach is based on the hybrid finite element-boundary integral-multilevel fast multipole algorithm (FE-BI-MLFMA). Unlike the conventional single-domain FE-BI-MLFMA, the whole domain of the antenna array with radome is separated into many disconnected domains. A large free space area unavoidable in the single-domain FE-BI-MLFMA is eliminated in this multi-domain FE-BI-MLFMA formulation, thus the number of unknowns is greatly reduced in the presented multi-domain FE-BI-MLFMA approach. Different from the single-domain FE-BI-MLFMA, many integral equations are required in this multi-domain FE-BI-MLFMA. The numerical experiment shows that the presented multi-domain FE-BI-MLFMA is more efficient than the single-domain one while maintaining the same accuracy. A whole complicated system of a slotted-waveguide array with radome mounted on an aircraft is analyzed to further demonstrate the generality and capability of the presented multi-domain FE-BI-MLFMA.

1. INTRODUCTION

Electromagnetic radiation analysis of antenna array with radome on electrically large complex platform has become more and more important for modern communication and radar system design. To satisfy the electromagnetic, aerodynamic, structural, and environmental requirements, a radome is usually employed for the purpose of protection and mechanical stability. The presence of radome may affect greatly the radiation characteristics of an antenna due to the induced currents. Hence the radiation characteristics analysis for antenna with radome system is important for practical design.

There are many methods for solving this kind of problems, such as the high frequency asymptotic methods, full-wave numerical methods and the hybrid full-wave and high frequency methods [1–14]. Full-wave numerical methods have been well developed to analyze the slotted-waveguide antenna [5–9]. However, due to large computation resources required, they usually are applied to analyze radiation by electrically small radome/antenna problems. For the scattering or radiation analysis of electrically large three-dimensional problems in electromagnetic engineering, the high frequency method is usually employed to achieve efficient calculation, such as Ray Tracing (RT), Physical Optics (PO), hybrid full-wave and high frequency methods [10–14]. But when these methods are applied to compute the radiation by a large antenna array with radome on a large aircraft, they usually become inefficient due to multi-scale, multi-regional connectivity and multi-materials problems. More importantly, the computation accuracy of high frequency methods is not promised. Fast and accurate analysis of the large slotted-waveguide arrays with radome on a large aircraft is still a great challenge.

The FE-BI-MLFMA has shown to be a flexible, accurate and efficient method for dealing with scattering/radiation problems [15–18]. Recently, a domain decomposition method is presented for

Received 20 August 2015, Accepted 13 October 2015, Scheduled 26 October 2015
* Corresponding author: Xin-Qing Sheng (xsheng@bit.edu.cn).
The authors are with the Center for Electromagnetic Simulation, School of Information Science and Technology, Beijing Institute of Technology, Beijing 100081, China.

analyzing electromagnetic problems involving multiple separable scatterers such as an antenna array in [19]. But the solution domain of FE-BI-MLFMA in [19] is a connected single domain, the large free space area in the solution domain is unavoidable. In this paper, we present an accurate and efficient multi-domain FE-BI-MLFMA approach for large slotted-waveguide antenna arrays with a radome on a large aircraft. The single connected domain of an antenna array with radome in the original FE-BI-MLFMA in [19] is first separated into many disconnected domains. Then each domain is simulated with the FEM as usual. To establish the relation of electric and magnetic fields at the boundary of each domain, we establish two integral equations. One is the integral equation established on the exterior surface of the radome and the large aircraft. The other is one established on the interior surface of the radome and the surfaces of all radiation units of the antenna array. Thus the free space region unavoidable in the single-domain FE-BI-MLFMA is not needed in the multi-domain FE-BI-MLFMA, a large number of unknowns can be reduced. Furthermore, our numerical experiments show that the multi-domain FE-BI approach has faster convergent solution than the single-domain one. The radiation characteristics of a large X-band slotted-waveguide antenna array containing eighteen waveguides with a radome is computed and analyzed. A challenging problem of a slotted-waveguide array with radome mounted on a large aircraft is analyzed to further demonstrate the generality and capability of the presented multi-domain FE-BI-MLFMA.

2. COMPUTATIONAL ALGORITHM

Consider the radiation problem of multiple disconnected antenna arrays with a radome as shown in Fig. 1. The radome is a spheroidal dielectric shell with relative permittivity ε_r and permeability μ_r, the array with multi slotted-waveguides is enclosed by a radome.

In the conventional FE-BI-MLFMA, the solution region is directly divided into the interior region and the exterior region. As shown in Fig. 1(a), for the interior region, there is only a single-domain bounded by the outer surface of the radome. The interior region not only includes the volume region of each antenna array and the radome, but also includes the free space region bounded by the outer surface of each antenna array and the inner surface of the radome. A large amount of additional FEM unknowns are required due to the free-space region, which results in a large computation resource and a limitation of the problem size. To overcome this bottleneck, we present an efficient multi-domain FE-BI-MLFMA approach as shown in Fig. 1(b). For each slotted-waveguide, its relative permittivity and permeability are $\tilde{\varepsilon}_{i,r}$, $\tilde{\mu}_{i,r}$ $(i = 1, N)$ respectively.

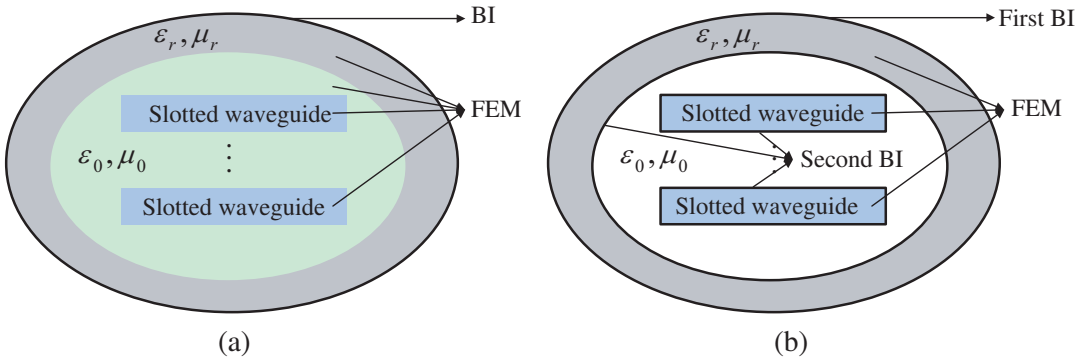

Figure 1. The single-domain and multi-domain FE-BI-MLFMA scheme for arrays with radome. (a) Single-domain FE-BI-MLFMA. (b) Multi-domain FE-BI-MLFMA.

To be more specific, consider the radiation problem of a large slotted-waveguide antenna with a dielectric radome, the computational model for analysis is shown in Fig. 2. For the mth $(m = 1, N)$ slotted-waveguide, its surface is denoted as S_m. According to the FE-BI-MLFMA presented in [17], the solution region is directly divided into the interior region and the exterior region by the surface of S_m. The excited source is placed on the fed edges in each single slotted-waveguide interior region, the

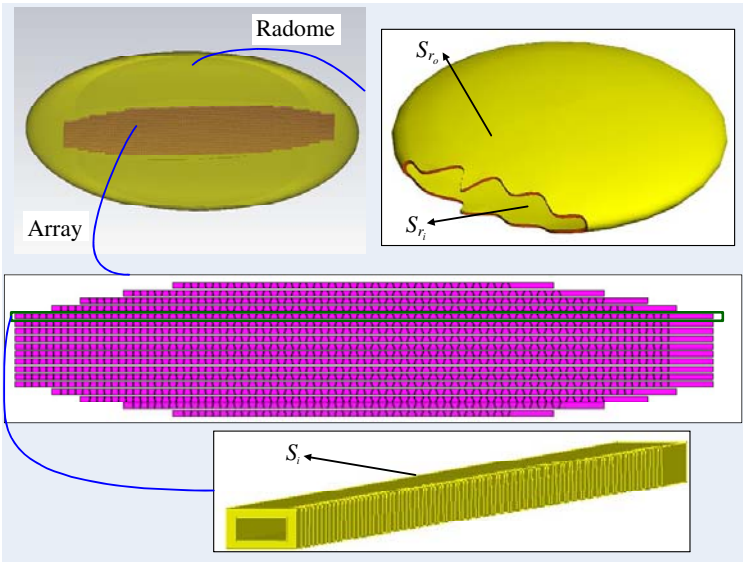

Figure 2. Model for large slotted-waveguide antenna array with radome.

fields in the interior region V_m of a single slotted-waveguide antenna are formulated into an equivalent variational problem with the functional given by:

$$F_m(\mathbf{E}_m) = \frac{1}{2}\iiint_{V_m}\left[(\nabla\times\mathbf{E}_m)\cdot\left([\tilde{\mu}_{m,r}]^{-1}\nabla\times\mathbf{E}_m\right) - k_0^2\mathbf{E}_m\cdot[\tilde{\varepsilon}_{m,r}]\cdot\mathbf{E}_m\right]dV + jk_0\iint_{S_m}\left(\mathbf{E}_m\times\bar{\mathbf{H}}_m\right)\cdot\hat{n}_m dS + jk_0Z_0\iiint_{V_m}\mathbf{J}_m^{inp}\cdot\mathbf{E}_m dV \quad (1)$$

where k_0 is the free-space wavenumber, $\bar{\mathbf{H}}_m = Z_0\mathbf{H}_m$, Z_0 the free-space intrinsic impedance, V_m the volume enclosed by S_m, and $\hat{n}_m$ the outward unit vector normal to S_m. The short current probe oriented in the z-direction and located at $(x_f,\, y_f)$ can be modeled as:

$$\mathbf{J}^{inp} = \hat{z}I_0\delta\left(x - x_f,\, y - y_f\right)e^{-jk\varphi} \quad (2)$$

The volume V_r of the dielectric radome is enclosed by the inner surface S_{r_i} and outer surface S_{r_o} of the radome, shown in Fig. 2. Similarly, the fields in V_r can be also formulated into an equivalent variational problem with the similar functional of (1) except that the last term of excitation is omitted.

The relation of electric and magnetic fields at the surface of radome and each slotted-waveguide can be established by two integral equations. One is the integral equation established at the outer surface of radome. The other is one established at the inner surface of radome and the surfaces of all slotted-waveguides. These two integral equations can be formulated as the following same form of the combined field integral equation (CFIE) except that the integral areas in operators $\mathbf{L}_x$ and $\mathbf{K}_x$ are different

$$\pi_{t_r}\left\{-\frac{1}{2}\mathbf{E} + \sum_{m=1}^{N}\left[\mathbf{L}_m(\hat{n}_m\times\bar{\mathbf{H}}_{S_m}) - \mathbf{K}_m(\mathbf{E}_{S_m}\times\hat{n}_m)\right] + \mathbf{L}_r(\hat{n}_r\times\bar{\mathbf{H}}_{S_r}) - \mathbf{K}_r(\mathbf{E}_{S_r}\times\hat{n}_r)\right\}$$
$$+\pi_{\times_r}\left\{-\frac{1}{2}\bar{\mathbf{H}} + \sum_{m=1}^{N}\left[\mathbf{L}_m(\mathbf{E}_{S_m}\times\hat{n}_m) + \mathbf{K}_m(\hat{n}_m\times\bar{\mathbf{H}}_{S_m})\right] + \mathbf{L}_r(\mathbf{E}_{S_r}\times\hat{n}_r) + \mathbf{K}_r(\hat{n}_r\times\bar{\mathbf{H}}_{S_r})\right\} = 0 \quad (3)$$

where

$$\pi_{t_r}(\cdot) = \hat{n}_r\times(\cdot)\times\hat{n}_r$$
$$\pi_{\times_r}(\cdot) = \hat{n}_r\times(\cdot)$$

$$\begin{aligned}\mathbf{L}_x(\mathbf{X}) &= -jk_0 \int\limits_{S_x} \left[\mathbf{X}(\mathbf{r}') + \frac{1}{k_0^2}\nabla' \cdot \mathbf{X}(\mathbf{r}')\nabla\right] G_0(\mathbf{r},\mathbf{r}')dS' \\ \mathbf{K}_x(\mathbf{X}) &= -\int\limits_{S_x} \mathbf{X}(\mathbf{r}') \times \nabla G_0(\mathbf{r},\mathbf{r}')dS'\end{aligned} \tag{4}$$

Using the standard FEM and MoM to discretize (1) and (3) yields the FE-BI matrix equation of (5), where $\mathbf{K}$ and $\mathbf{B}$ are the sparse FEM matrices, $\mathbf{P}_{fk}$ and $\mathbf{Q}_{fk}$ $(k = 1, 2, \ldots, N, r_i, r_o)$ are the dense matrices from the first integral equation established at the inner surface of the radome and surfaces of all slotted waveguides, $\mathbf{P}_{sr_o}$ and $\mathbf{Q}_{sr_o}$ are the dense matrices from the second integral equation established at the outer surface of the radome, $\mathbf{R}_m$ and $\mathbf{R}_r$ denotes the projection Boolean matrix between the local BI degrees of freedom (DOFs) and the local FEM degrees of freedom (DOFs) of the mth slotted waveguide and radome, respectively. $\bar{H}_s = Z_0 H_s$, Z_0 is the free-space impedance.

$$\begin{bmatrix} \mathbf{K}_1 & 0 & 0 & 0 & \mathbf{R}_1\mathbf{B}_1 & 0 & 0 & 0 & 0 \\ 0 & \ddots & 0 & 0 & 0 & \ddots & 0 & 0 & 0 \\ 0 & 0 & \mathbf{K}_N & 0 & 0 & 0 & \mathbf{R}_N\mathbf{B}_N & 0 & 0 \\ 0 & 0 & 0 & \mathbf{K}_r & 0 & 0 & 0 & \mathbf{R}_{r_i}\mathbf{B}_{r_i} & \mathbf{R}_{r_o}\mathbf{B}_{r_o} \\ \mathbf{P}_{f1}(\mathbf{R}_1)^T & \ldots & \mathbf{P}_{fN}(\mathbf{R}_N)^T & \mathbf{P}_{fr_i}(\mathbf{R}_{r_i})^T & \mathbf{Q}_{f1} & \ldots & \mathbf{Q}_{fN} & \mathbf{Q}_{fr_i} & \mathbf{Q}_{fr_o} \\ 0 & 0 & 0 & \mathbf{P}_{sr_o}(\mathbf{R}_{r_o})^T & 0 & 0 & 0 & 0 & \mathbf{Q}_{sr_o} \end{bmatrix} \begin{bmatrix} E_1 \\ \vdots \\ E_N \\ E_r \\ \bar{H}_{s_1} \\ \vdots \\ \bar{H}_{s_N} \\ \bar{H}_{s_{r_i}} \\ \bar{H}_{s_{r_o}} \end{bmatrix}$$

$$= \begin{bmatrix} f_1 \\ \vdots \\ f_N \\ 0 \\ 0 \\ 0 \end{bmatrix} \tag{5}$$

The equation system of (5) is solved by using the iterative solvers such as GMRES. The MLFMA is employed to speed up matrix-vector multiplication, which is the key step of GMRES. In this paper, to further improve the efficiency, the sparse solver of the multifrontal direct method [20] is first employed to factorize the FEM matrix $[\mathbf{K}_m]$ to obtain the expression of E_m by using H_{s_m}, then the finite element tearing and tearing and interconnecting method (FETI) [17] is employed to handle the FEM matrix of the radome before solving (5).

It is worth to point out the above presented formulation can be extended to general cases in a straightforward way. For example, if the radome is multilayered, not homogeneous, we can establish an integral equation for every interface between layers. Thus, we obtain an equation system with more than two integral equations.

3. NUMERICAL RESULTS

A series of numerical experiments are investigated in this section. All the computations are performed on a parallel computer platform *Liuhui*-II at the Center for Electromagnetic Simulation, Beijing Institute of Technology. It has 10 nodes, each node has 96 GB memory, 2 Intel X5650 2.66 GHz CPUs, and each CPU has 6 cores.

A ten-slot waveguide array with radome is first computed to investigate the convergence performance and accuracy of the presented multi-domain DDA-FE-BI-MLFMA approach. We employ a rugby-like ellipsoid radome to enclose the slotted-waveguide array. As shown in Fig. 3, the long semi-axis of radome is 13.3λ, the thickness is 0.6λ, and the relative permittivity is $\varepsilon_r = 2.0 - j1.0$. The radiation patterns of the array-radome are calculated by using our presented multi-domain and the conventional single-domain algorithms. The comparison of normalized co-polarization E-plane and H-plane radiation

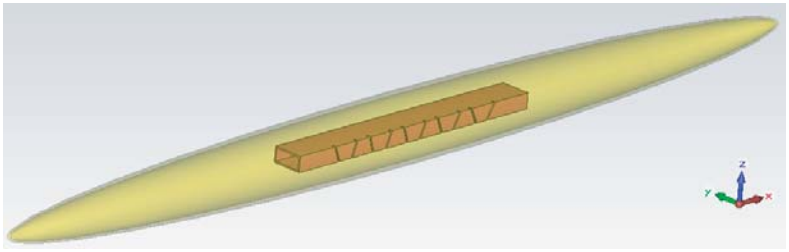

Figure 3. Model for ten-slot waveguide antenna with radome.

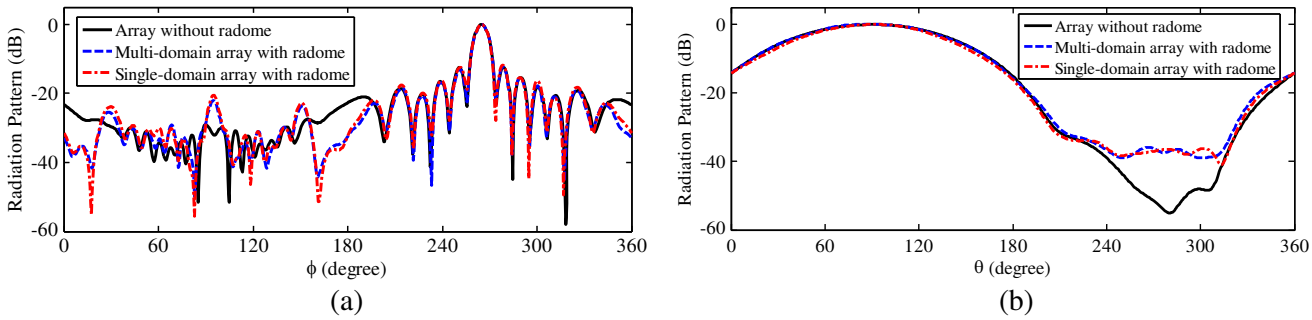

Figure 4. Radiation patterns for ten-slot waveguide antenna with radome at 10 GHz. (a) Co-Pol. in E-plane. (b) Co-Pol. in H-plane.

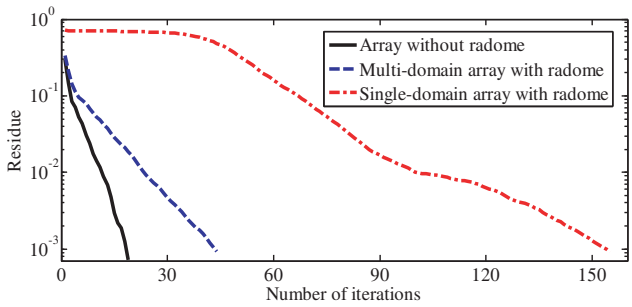

Figure 5. Convergence of the iterative solution of the ten-slots waveguide antenna with radome under different domains mesh.

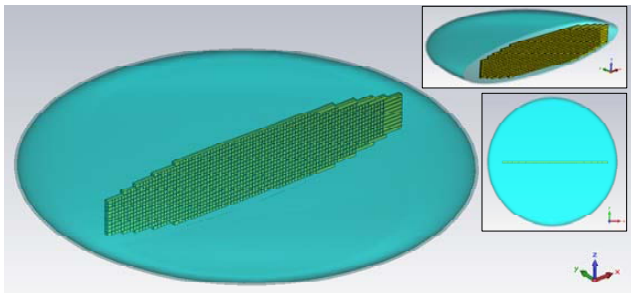

Figure 6. The large slotted-waveguide array with radome.

patterns of the array is shown in Fig. 4, demonstrating that the multi-domain DDA-FE-BI-MLFMA has good accuracy.

Figure 5 shows the convergence history of the iterative solution of the ten-slot waveguide antenna with radome under different algorithms. The results show that the multi-domain approach has faster convergence than the single-domain approach. The numbers of unknowns are 2,717,248(FEM)/242,679(BI) in the multi-domain approach and 4,524,260(FEM)/146,550(BI) in the single-domain one. The total memory requirements are 21 GB and 38 GB, and the total CPU times are 46 minutes and 112 minutes respectively in the multi-domain and single-domain approaches. In this calculation, we employ 8 CPU cores.

Then a large slotted-waveguide array with an oblate ellipsoid radome, as shown in Fig. 6, is computed to analyze the impact of radome on the radiation characteristics. The large array contains 18 slotted waveguides and total 1416 slot units. These 18 slotted waveguides are equally divided into two groupsgroup A and group B. The group A is symmetry to the group B along the middle line of the

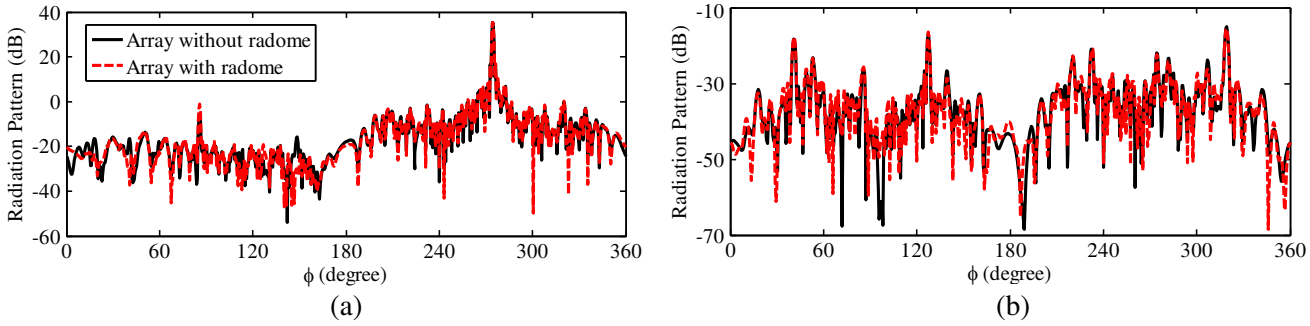

Figure 7. E-plane radiation patterns for large slotted-waveguide array with radome at 10 GHz. (a) Co-polarization. (b) Cross-polarization.

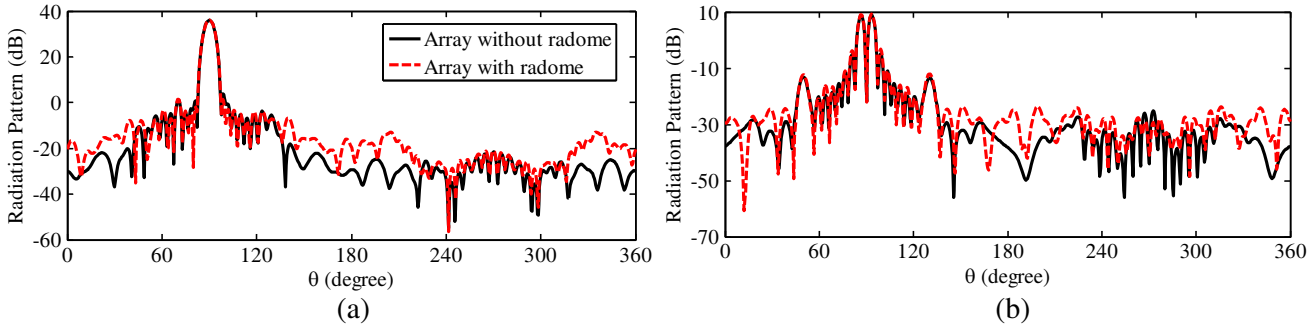

Figure 8. H-plane radiation patterns for large slotted-waveguide array with radome at 10 GHz. (a) Co-polarization. (b) Cross-polarization.

array in xoz plane. The inclination direction for each slot is inversed to its adjacent ones. The BJ100 waveguide (22.86×10.16 mm) is chosen for each antenna, the working frequency band of the dominant mode ranges from 8.2 GHz to 12.5 GHz. The working central frequency of the array is 10 GHz. The vertical spacing among the waveguides is 5.2 mm. To achieve high gain and low side-lobe performance, the fed phase for each slotted-waveguide is strictly inversed to the adjacent ones. Furthermore, the fed phase for slotted-waveguide in the group A is strictly inversed to that for the symmetrical slotted-waveguide in the group B. A single layer dielectric oblate ellipsoid radome with its long semi-axis of 43.3λ and short semi-axis of 8.7λ is designed for the array. The radome has a thickness of 0.1λ and a relative permittivity of $\varepsilon_r = 2.0 - j1.0$.

The two orthogonal polarization radiation patterns in E-plane and H-plane are calculated by using the presented multi-domain approach, and are shown in Fig. 7 and Fig. 8. The results show the impact of the radome on the radiation pattern of the array. The interaction between array and radome greatly affects the radiation patterns in the H-plane, and has a large elevation of side-lobe envelope due to the large variation of the radome curvature in the yoz plane, but little in the E-plane due to the unchanged curvature of the radome in the xoy plane. The computational resources required in this calculation are listed in Table 1.

To demonstrate the generality and capability of the presented multi-domain FE-BI-MLFMA, a more challenging problem is analyzed, as shown in Fig. 9. The above slotted-waveguide array with radome is mounted on a large aircraft. The aircraft is 14.25 m long, and 16 m wide. The array is mounted 2.1 m high from the top of the aircraft, and 7.36 m away from the nose of the aircraft. We consider two cases. The case 1 is that the main bean of the array faces to the nose. The case 2 is that the main bean of the array faces to the tail. Fig. 10 shows the effect of the aircraft to the radiation patterns of the slotted-waveguide array. The computational resources required in this calculation are listed in Table 2.

Table 1. Computational resources for calculating.

Unknowns	13,211,715(FEM)/7,034,247(BI)
CPU cores	21
Iteration Residue	$1.0E-03$
Iteration Number	380
Total Memory	210 G
Total Time	10 h 29 m

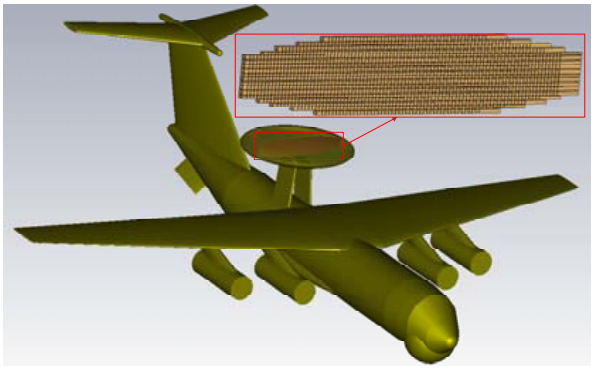

Figure 9. Slotted-waveguide array with radome mounted on an aircraft.

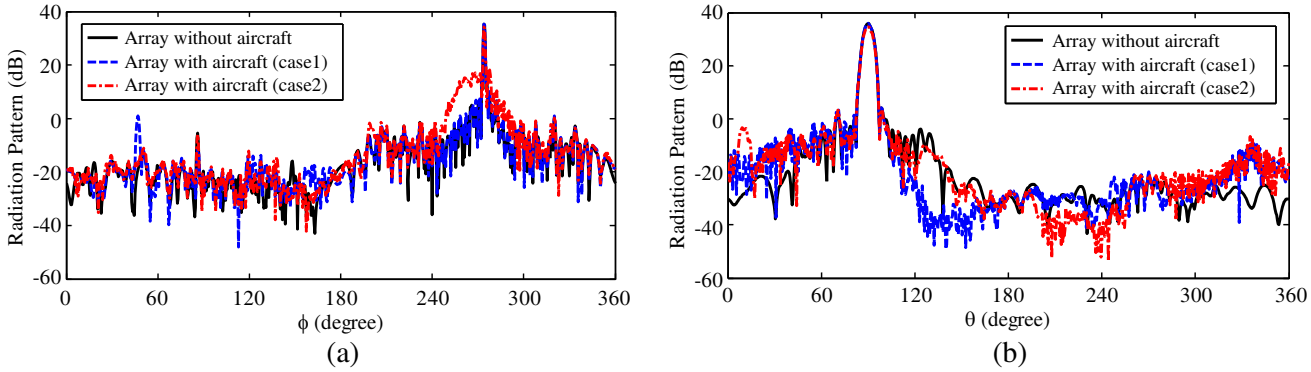

Figure 10. Radiation patterns for large slotted-waveguide array with radome mounted on an aircraft at 10 GHz. (a) E-plane. (b) H-plane.

Table 2. Computational resources for slotted-waveguide array with radome mounted on an aircraft.

Unknowns	13,211,715(FEM)/40,070,181(BI)
CPU cores	50
Iteration Residue	$1.0e-03$
Iteration Number	530
Total Memory	590 G
Total Time	19 h 40 m

4. CONCLUSION

An efficient multi-domain FE-BI-MLFMA approach is presented for large slotted-waveguide antenna arrays with radome in this paper. The comparison of the computed results by the presented multi-domain and conventional single-domain FE-BI-MLFMA validates that the presented approach is fast and accurate for analysis of slotted-waveguide arrays with radome. The effect of the radome is analyzed to the radiation patterns of a large slotted-waveguide array antenna. A challenging problem of a large slotted-waveguide array with radome mounted on a large aircraft is computed to further demonstrate the efficiency and capability of the presented approach.

ACKNOWLEDGMENT

This work is partially supported by the National Basic Research Program (973) under Grant No. 61320602 and No. 61327301, the 111 Project of China under the Grant B14010, and the NSFC under Grant 61421001.

REFERENCES

1. Gordon, R.-K. and R. Mittra, "Finite element analysis of axisymmetric radomes," *IEEE Transactions on Antennas and Propagation*, Vol. 41, No. 7, 975–981, 1993.
2. Arvas, E. and S. Ponnapalli, "Radar cross section of a small radome of arbitrary shape," *IEEE Transactions on Antennas and Propagation*, Vol. 37, No. 5, 655–658, 1989.
3. Gao, X.-J. and L.-B. Felsen, "Complex ray analysis of beam transmission through two-dimensinal radomes," *IEEE Transactions on Antennas and Propagation*, Vol. 33, No. 9, 963–975, 1985.
4. Shifflett, J.-A., "CADDRAD: A physical optics radar/radome analysis code for arbitrary 3D geometries," *IEEE Transactions on Antennas and Propagation*, Vol. 39, No. 6, 73–79, 1997.
5. Stevenson, A.-F., "The theory of slots in rectangular waveguides," *J. Appl. Phys.*, Vol. 19, 24–38, Jan. 1948.
6. Oliner, A.-A., "The impedance properties of narrow radiating slots in the broad face of rectangular waveguide," *IEEE Transactions on Antennas and Propagation*, Vol. 5, 4–20, Jan. 1957.
7. Krant, E.-A., J.-C. Olinier, and J.-B. West, "FDTD solution of Maxwell's equations for an edge slot penetrating adjacent broadwalls of finite wall thickness waveguide," *IEEE Transactions on Antennas and Propagation*, Vol. 42, 1646–1648, Dec. 1994.
8. Prakash, V.-V.-S., S. Christopher, and N. Balakrishnan, "Method-of-Moments analysis of the narrow-wall slot array in a rectangular waveguide," *IEE Proc., Microw. Antennas Propagat.*, Vol. 147, 242–246, Jun. 2000.
9. Young, J.-C., J. Hirokawa, and M. Ando, "Analysis of a rectangular waveguide, edge slot array with finite wall thickness," *IEEE Transactions on Antennas and Propagation*, Vol. 55, 812–819, Mar. 2007.
10. Zhao, W.-J., Y.-B. Gan, C.-F. Wang, et al., "Coupled IE-PO method for analysis of antenna radiation patterns in the presence of a large 3D radome," *IEEE Antennas & Propagation Society International Symposium*, 695–698, 2004.
11. Zhao, X.-W., Y. Zhang, H.-W. Zhang, D. Garcia-Donoro, S.-W. Ting, T. K. Sarkar, and C.-H. Liang, "Parallel MoM-PO method with out-of-core technique for analysis of complex arrays on electrically large platforms," *Progress In Electromagnetics Research*, Vol. 108, 1–21, 2010.
12. Nie, X.-C., Y.-B. Gan, N. Yuan, C.-F. Wang, and J. L.-W. Li, "An efficient hybrid method for analysis of slot arrays enclosed by a large radome," *Journal of Electromagnetic Waves and Applications*, Vol. 20, No. 2, 249–264, 2006.
13. Hu, B., X.-W. Xu, M. He, and Y. Zheng, "More accurate hybrid PO-MoM analysis for an electrically large antenna-radome structure," *Progress In Electromagnetics Research*, Vol. 92, 255–265, 2009.
14. Meng, H.-F. and W.-B. Dou, "Fast analysis of electrically large radome in millimeter wave band with fast multipole acceleration," *Progress In Electromagnetics Research*, Vol. 120, 371–385, 2011.

15. Eibert, T. and V. Hansen, "Calculation of unbounded field problems in free space by a 3-D FEM/BEM-hybrid approach," *Journal of Electromagnetic Waves and Applications*, Vol. 10, No. 1, 61–77, 1996.
16. Sheng, X.-Q., J.-M. Song, C.-C. Lu, and W.-C. Chew, "On the formulation of hybrid finite-element and boundary-integral method for 3D scattering," *IEEE Transactions on Antennas and Propagation*, Vol. 46, 303–311, Mar. 1998.
17. Liu, J. and J.-M. Jin, "A highly effective preconditioner for solving the finite element-boundary integral matrix equation for 3-D scattering," *IEEE Transactions on Antennas and Propagation*, Vol. 50, 1212–1221, Sep. 2002.
18. Yang, M.-L., H.-W. Gao, and X.-Q. Sheng, "Parallel domain-decomposition-based algorithm of hybrid FE-BI-MLFMA method for 3-D scattering by large inhomogeneous objects," *IEEE Transactions on Antennas and Propagation*, Vol. 50, No. 2, 4675–4684, Sep. 2013.
19. Xue, M.-F. and J.-M. Jin, "A hybrid conformal/nonconformal domain decomposition methods for solving large-scale multi-region electromagnetic problems," *IEEE Transactions on Antennas and Propagation*, Vol. 62, No. 4, 2009–2021, Apr. 2014.
20. Amestoy, P.-R., I.-S. Duff, J. Koster, and J.-Y. L'Excellent, "A fully asynchronous multifrontal solver using distributed dynamic scheduling," *SIAM Journal of Matrix Analysis and Applications*, Vol. 23, 15–41, Jan. 2001.